

Peritectic Solidification Path of the $\text{La}(\text{Fe},\text{Si})_{13}$ Phase in Dual-Phase Directionally Solidified La-Fe-Si Magnetocaloric Alloys



LIANG YANG, ZHENNI ZHOU, JIANGRUI QIAN, XUAN GE, JUN LI, QIAODAN HU, and JIANGUO LI

NaZn_{13} -type $\text{La}(\text{Fe},\text{Si})_{13}$ alloy is a promising magnetocaloric material for solid refrigeration. Currently, several days of high-temperature annealing are typically required to transform both the α -Fe phase and LaFeSi phase to a $\text{La}(\text{Fe},\text{Si})_{13}$ phase by diffusion. However, no bulk casting has yet been reported. In this study, directional solidification is used to prepare $\text{LaFe}_{11.6}\text{Si}_{1.4}$ alloys with a dual-phase microstructure consisting of α -Fe and LaFeSi phases. It was found that the volume fraction of $\text{La}(\text{Fe},\text{Si})_{13}$ phase in directionally solidified $\text{LaFe}_{11.6}\text{Si}_{1.4}$ alloys can be increased to ~62 pct. It was also found that the volume fraction of the $\text{La}(\text{Fe},\text{Si})_{13}$ phase is dependent primarily on the temperature gradient at different growth rates, which can be the result of their wide temperature range between solidus and liquidus. A significant Si segregation was observed in directionally solidified $\text{LaFe}_{11.6}\text{Si}_{1.4}$ alloys. Furthermore, the solidification path was discussed, focusing on the volume fraction increase of the $\text{La}(\text{Fe},\text{Si})_{13}$ phase by directional solidification.

DOI: 10.1007/s11661-017-4179-6

© The Minerals, Metals & Materials Society and ASM International 2017

I. INTRODUCTION

SOLID refrigeration has the potential to replace conventional gas compression/expansion refrigeration as a result of the increasing environmental concern.^[1-3] In this case, La-Fe-Si alloy, with NaZn_{13} -type $\text{La}(\text{Fe},\text{Si})_{13}$ phase, has been reported as a promising candidate for magnetic refrigerants.^[4,5] $\text{La}(\text{Fe},\text{Si})_{13}$ alloy exhibits a giant magnetocaloric effect (MCE, which refers to the heating or cooling of magnetic materials due to a varying magnetic field) due to a magnetic field-induced, first-order itinerant electron metamagnetic (IEM) transition above the Curie temperature (T_C).^[6] $\text{La}(\text{Fe},\text{Si})_{13}$ alloy displays a small hysteresis and an isotropic magnetovolume effect accompanied by the phase transition.^[7-9] These properties are beneficial for a cyclic use of La-Fe-Si alloys because of the existing giant magnetocaloric effect. Several attempts have been made to improve the properties of $\text{La}(\text{Fe},\text{Si})_{13}$ magnetocaloric alloys, such as partial element substitution, atom

insertion, and applying extra pressure by using hydrogenation.^[10-14]

NaZn_{13} -type $\text{La}(\text{Fe},\text{Si})_{13}$ phase (1:13 phase) is a peritectic phase that is formed by a peritectic solidification reaction. However, the 1:13 phase was not observed using conventional techniques, such as arc-melting. Instead, the as-cast La-Fe-Si alloys show a two-phase structure composed of α -(Fe,Si) and La-Fe-Si (Cu_2Sb -type: P4/nmm) phases. According to the phase diagram, during equilibrium solidification, the α -Fe phase (primary phase) dendrites first grow from the liquid. Once the prime phase forms, a peritectic reaction with the surrounding liquid forms the peritectic phase. Once the peritectic phase appears at the junction of the prime phase and surrounding liquid, the peritectic solidification will be blocked.^[15] It has been reported that a dual-phase structure containing both α -Fe and $\text{La}(\text{Fe},\text{Si})_{13}$ shows an enhanced thermal conductivity and mechanical property compared with the single-phase structure.^[16] The existence of the α -Fe phase can improve the mechanical properties, particularly, the ductility of La-Fe-Si alloys due to the internal brittleness of the $\text{La}(\text{Fe},\text{Si})_{13}$ phase. However, this dual-phase microstructure is achieved by high-temperature annealing of the non-stoichiometric $\text{La}(\text{Fe},\text{Si})_{13}$ alloy for an extended period of time.^[16] To our knowledge, bulk casting of the $\text{La}(\text{Fe},\text{Si})_{13}$ alloy is currently unavailable. Other novel methods have been used, such as melt-spun to refine the prime α -Fe phase and powder metallurgy

LIANG YANG, ZHENNI ZHOU, JIANGRUI QIAN, XUAN GE, JUN LI, QIAODAN HU and JIANGUO LI are with the School of Materials Science and Engineering, Shanghai Jiao Tong University, Shanghai 200240, People's Republic of China. Contact e-mails: li.jun@sjtu.edu.cn, qdhu@sjtu.edu.cn

Manuscript submitted November 18, 2016.

Article published online June 26, 2017

(HDSH) to insert H atoms; however, the alloys are prepared in powder and/or ribbon form.^[17–19]

Directional solidification has been used in the production of peritectic functional alloys and can tailor the microstructure, morphology, and oriented crystal growth, which has been reported for magnetic alloys such as Nd-Fe-B alloys.^[20] Additionally, it can influence the solidification path by controlling the temperature gradient and growth rate, as reported in our previous research of dual-phase (γ phase) Ni-Mn-In alloys.^[21] In this investigation, directional solidification is therefore used to fabricate the La-Fe-Si alloy, with a special focus on the volume fraction increase of the La(Fe,Si)₁₃ phase and the solidification path.

II. EXPERIMENT

Polycrystalline LaFe_{11.6}Si_{1.4} alloys were prepared by the arc-melt method using raw materials of La (with >99.5 pct purity), Fe (with >99.99 pct purity), and Si (with >99.9999 pct purity). To compensate for

volatilization, 5 pct extra of La was added. The button-shaped alloys were remelted, followed by suction cast in a copper mold to obtain rods 7 mm in diameter. The rods, after being cleaned and polished, were subsequently remelted and directionally grown in

Table I. Directionally Solidified LaFe_{11.6}Si_{1.4} Alloys Under Different Conditions

Alloy	Temperature Gradient (G_L , K/cm)	Crystal Growth Rate (R , $\mu\text{m/s}$)
G1000R100	1000	100
G1000R50	1000	50
G1000R15	1000	15
G600R100	600	100
G600R50	600	50
G600R15	600	15
G300R100	300	100
G300R50	300	50
G300R15	300	15

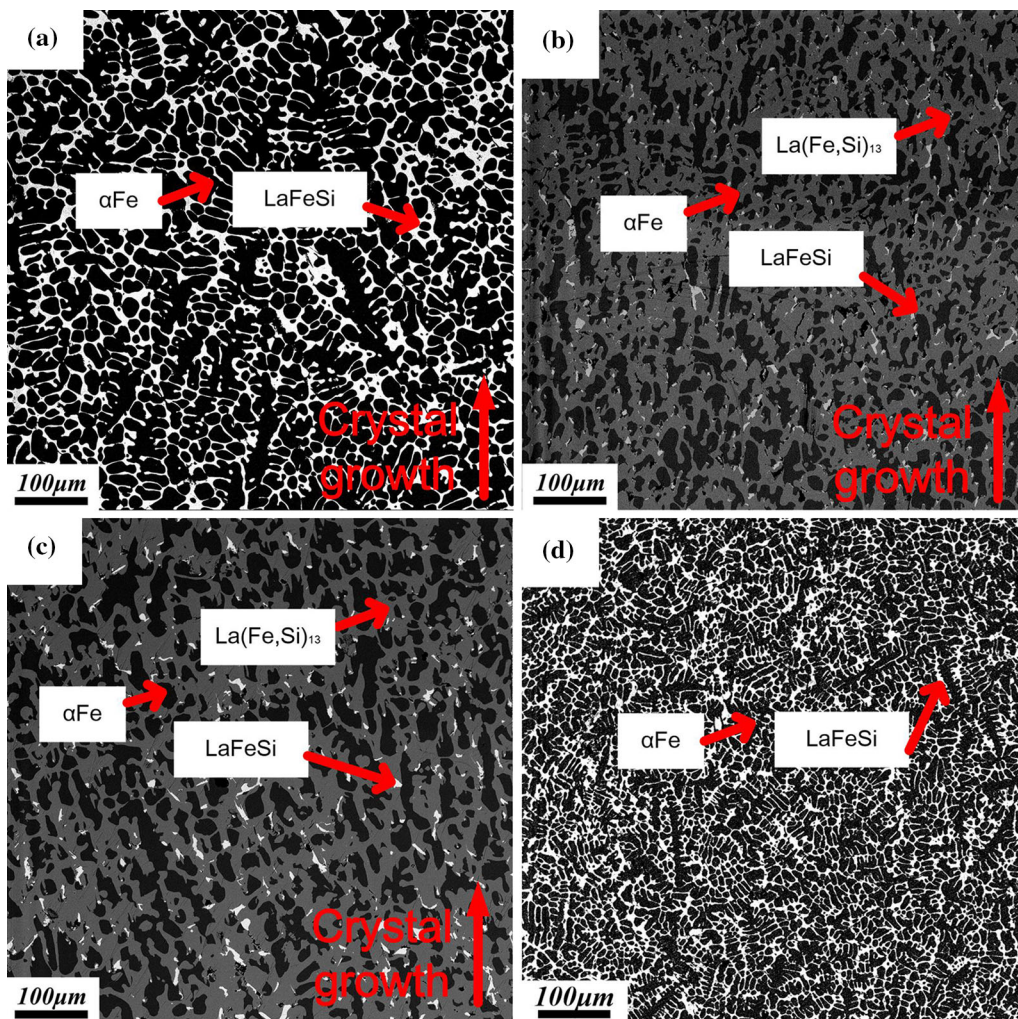


Fig. 1—SEM image (backscattered mode) of (a) G1000R100, (b) G1000R50, and (c) G1000R15 in the steady zone. For comparison, (d) is the SEM image (backscattered mode) of the as-cast LaFe_{11.6}Si_{1.4}. The black phase is α -Fe, the gray phase is La(Fe,Si)₁₃, and the white phase is LaFeSi.

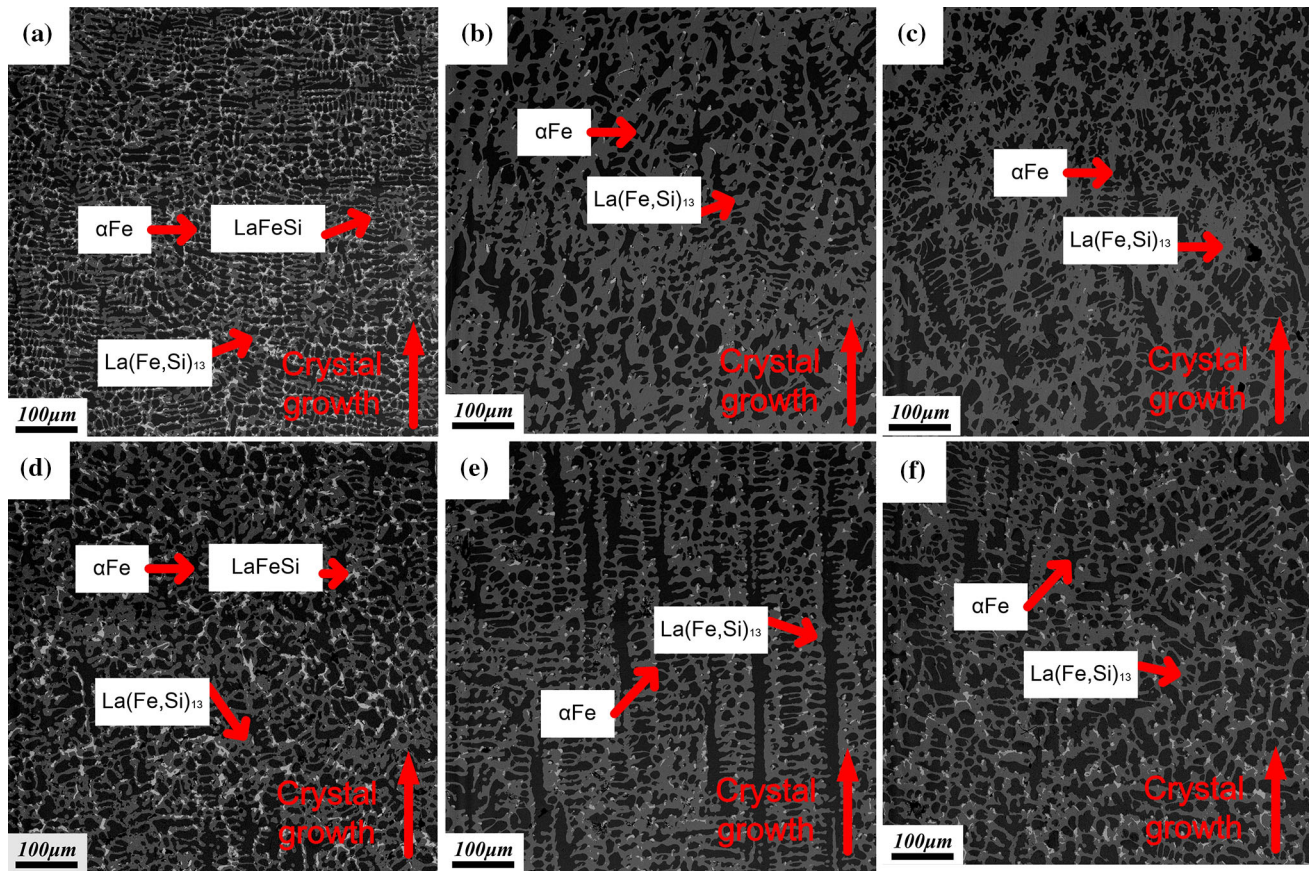


Fig. 2—SEM image (backscattered mode) of (a) G600R100, (b) G600R50, (c) G600R15, (d) G300R100, (e) G300R50, and (f) G300R15 in the steady zone. α -Fe phase, LaFeSi phase, and La(Fe,Si)_{13} phase are indicated.

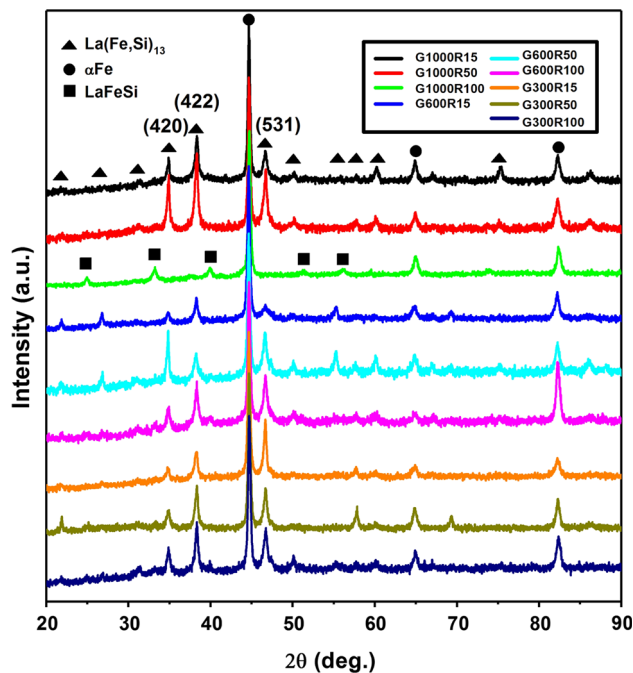


Fig. 3—XRD pattern for all directionally solidified $\text{LaFe}_{11.6}\text{Si}_{1.4}$ alloys. The figure shows that the La(Fe,Si)_{13} phase is present in all alloys except G1000R100.

alumina crucibles under different conditions, as shown in Table I. Directional solidification was carried out in a high-frequency induction vacuum zone melting liquid metal cooling (ZMLMC) furnace. Our previous research has shown an explanation for temperature gradient (G_L) and crystal growth rate (R).^[21]

Generally, the directionally solidified $\text{LaFe}_{11.6}\text{Si}_{1.4}$ rods include three parts along the growth direction, *i.e.*, the initial zone, steady zone, and last zone. In this investigation, only the steady zone is considered because the crystals grow relatively steady in this zone. Samples were taken from the longitudinal section of the directionally solidified rods. The microstructure was observed using scanning electron microscopy (SEM) in a backscattered mode. The compositional distribution of the directionally solidified rods was measured by energy-dispersive spectroscopy (EDS). Quantitative analysis of the volume fraction of interested phase is based on SEM images using Image-Pro Plus. The crystal structure was tested by X-ray diffraction (Ultima IV) using $\text{Cu K}\alpha$ radiation at a scan speed of 10 K/min.

III. RESULT

A. Morphology and Microstructure

In Figures 1(a) through (c), the morphology and microstructure of G1000R100, G1000R50, and

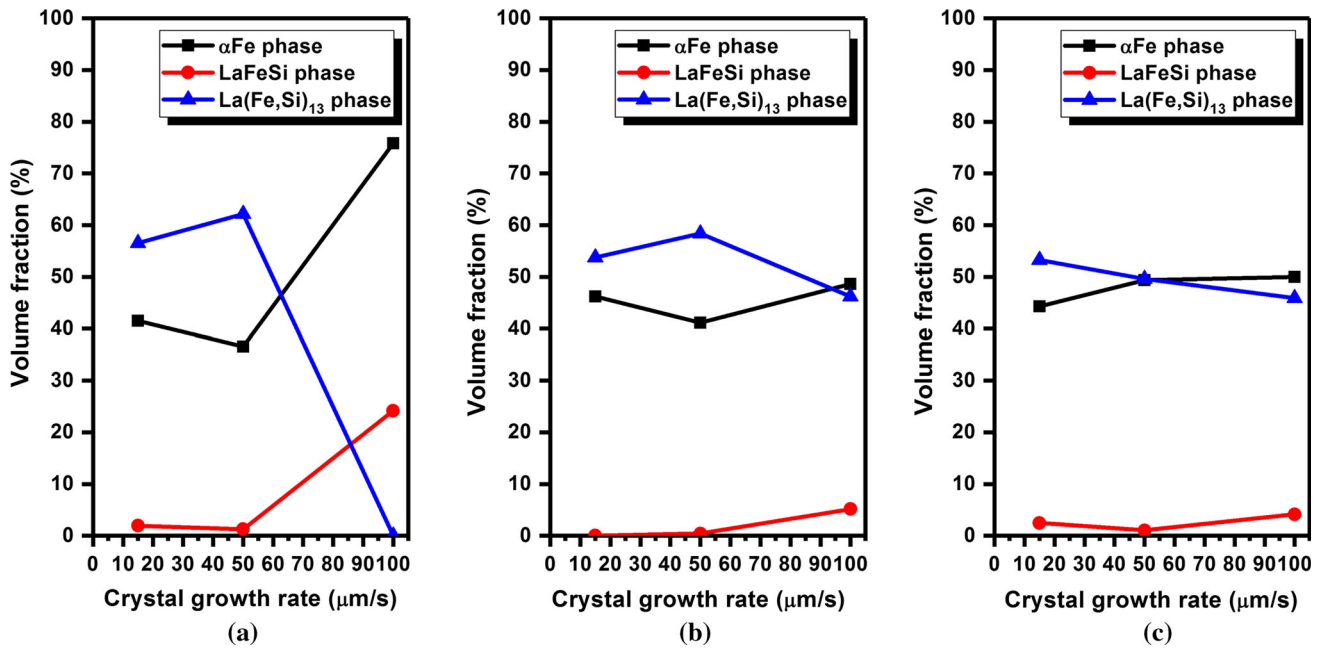


Fig. 4—Volume fraction of α -Fe phase, LaFeSi phase, and La(Fe,Si)₁₃ phase in directionally solidified LaFe_{11.6}Si_{1.4} alloys under different temperature gradients: (a) 1000 K/cm, (b) 600 K/cm, and (c) 300 K/cm.

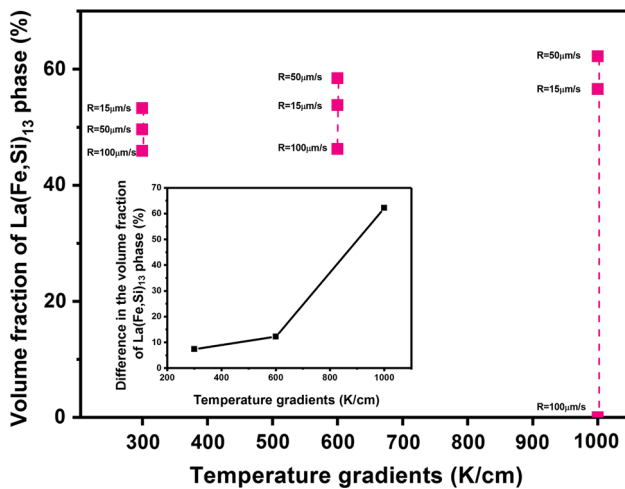


Fig. 5—The volume fraction of the La(Fe,Si)₁₃ phase vs the temperature gradients. The inset shows the influence of temperature gradients on the volume fraction of La(Fe,Si)₁₃ phase.

G1000R15 are revealed. For comparison, Figure 1(d) shows the microstructure of the corresponding arc-melt LaFe_{11.6}Si_{1.4} alloy. According to the EDS result (not shown here), the black, white, and gray phases are α -Fe, LaFeSi, and La(Fe,Si)₁₃, respectively. As expected, the 1:13 phase in the arc-melt alloy is not present (Figure 1(d)). For directional solidification, with a temperature gradient of 1000 K/cm and a grow speed of 100 $\mu\text{m/s}$, the 1:13 phase is also not present, as shown in Figure 1(a). For alloys G1000R50 and G1000R15, it is surprising to find that a large volume fraction of the La(Fe,Si)₁₃ phase appears. In all three directionally solidified alloys, the α -Fe phase shows a microstructure with an oriented growth direction. Furthermore, the

Table II. The Chemical Composition of La(Fe,Si)₁₃ Phase in all Obtained Directionally Solidified Alloys

Alloy	Chemical Composition of La(Fe,Si) ₁₃ Phase
G1000R100	/
G1000R50	La _{6.6} Fe _{79.5} Si _{13.9}
G1000R15	La _{6.9} Fe _{79.0} Si _{14.1}
G600R100	La _{6.7} Fe _{79.0} Si _{14.3}
G600R50	La _{6.7} Fe _{75.7} Si _{17.6}
G600R15	La _{7.0} Fe _{77.2} Si _{15.8}
G300R100	La _{7.2} Fe _{76.8} Si _{16.0}
G300R50	La _{7.0} Fe _{75.4} Si _{17.6}
G300R15	La _{6.3} Fe _{74.4} Si _{19.3}

α -Fe phase size of the directionally solidified LaFe_{11.6}Si_{1.4} is larger than the as-cast alloy. The α -Fe phase displays a thick and coarse microstructure in G1000R15, G1000R50, and G1000R100.

Alloys that were prepared with a relatively low temperature gradient (600 and 300 K/cm) were examined as well. Figure 2 shows the corresponding microstructure with alloys (Figures 2(a) through (c)) under the temperature gradient of 600 K/cm and alloys under the temperature gradient of 300 K/cm (Figures 2(d) through (f)). A large volume fraction of the 1:13 phase can be found in all alloys. In comparison with alloys prepared at $G = 1000$ K/cm, three phases are also present in directionally solidified alloys prepared at $G = 600$ K/cm, $R = 100$ $\mu\text{m/s}$, which are α -Fe, LaFeSi, and La(Fe,Si)₁₃ phases. However, the volume fraction of the LaFeSi phase in G600R50 and G600R15 alloys is rather low and displays a dual-phase microstructure. Compared with G1000R100, the size of the α -Fe phase in G600R100 is much smaller. α -Fe dendrites can be

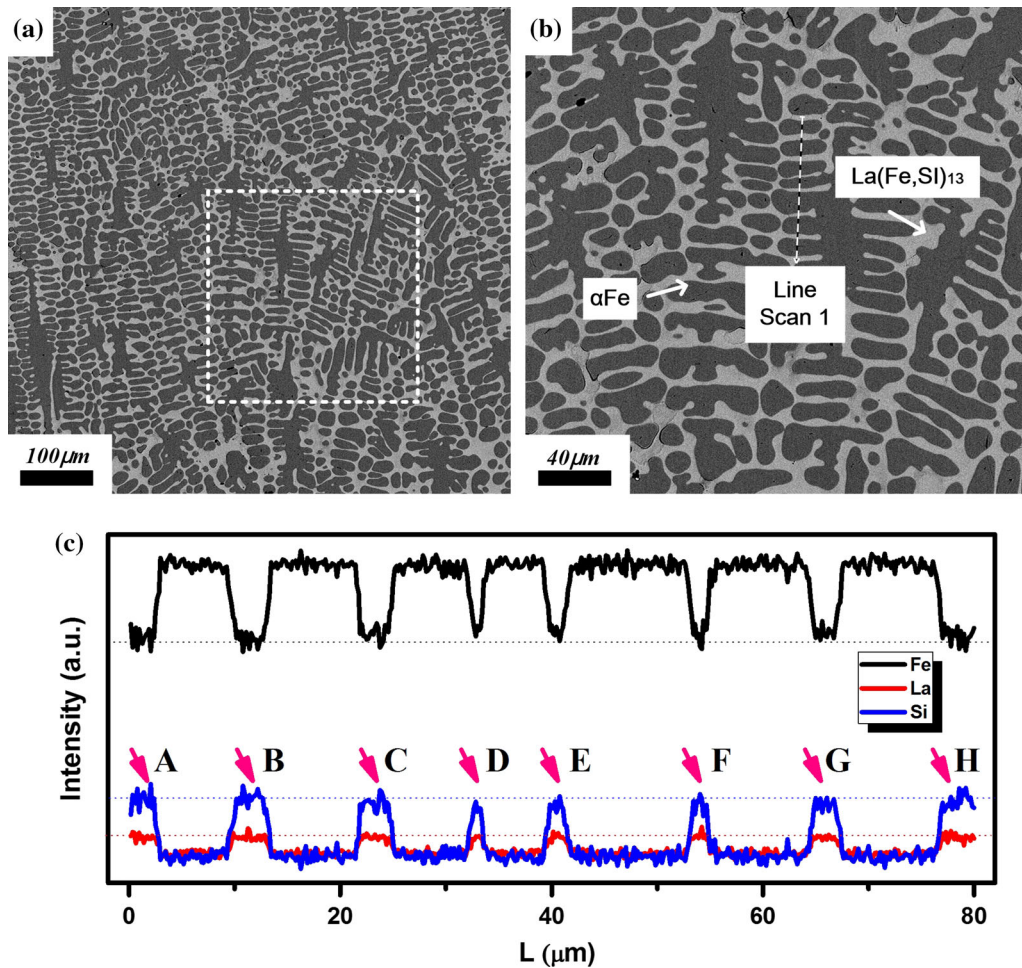


Fig. 6—EDS line scan through the prime phase α -Fe in G300R15 alloy. (a) a dual-phase microstructure consisting of α -Fe and $\text{La}(\text{Fe},\text{Si})_{13}$, and (b) the amplified figure of (a). (c) distribution of three elements La, Fe, and Si along the line scan. Arrow D-F appear as a ‘peak value,’ while the other arrow appear as a ‘platform value’.

clearly seen, and the prime dendrites are longer than those of the as-cast $\text{LaFe}_{11.6}\text{Si}_{1.4}$ (Figure 1(d)). When temperature gradient is reduced to 300 K/cm, G300R50 and G300R15 display a dual-phase microstructure similar to the alloys prepared with a temperature gradient of 600 K/cm. The size of α -Fe in these three alloys (G300R100, G300R50, and G300R15) is relatively large.

B. XRD Pattern of Directionally Solidified Alloys

To identify the crystal structure and determine whether there is a connection to the orientation between the prime phase α -Fe and the peritectic phase $\text{La}(\text{Fe},\text{Si})_{13}$, XRD analysis was carried out, as shown in Figure 3. The NaZn_{13} -type $\text{La}(\text{Fe},\text{Si})_{13}$ phase, which can exhibit a giant magnetocaloric effect, is clearly revealed in almost all of the directionally solidified alloys, except G1000R100. In addition, most directionally solidified $\text{LaFe}_{11.6}\text{Si}_{1.4}$ alloys appear as a dual-phase structure, except for alloys with high growth speeds, *i.e.*, G1000R100, G600R100, and G300R100. This is consistent with the morphology and microstructure observations.

For annealed $\text{La}(\text{Fe},\text{Si})_{13}$ alloys, the XRD peak (110) corresponding to α -Fe becomes weakened because of the phase transformation of α -Fe to $\text{La}(\text{Fe},\text{Si})_{13}$. However, the weakening is not seen in any directionally solidified $\text{LaFe}_{11.6}\text{Si}_{1.4}$ alloys. In Figure 3, peak (531) is shown to be weaker than peaks (422) and (420), which is different from annealed single-phase alloys, thus indicating a special connection between the prime phase α -Fe and the peritectic phase $\text{La}(\text{Fe},\text{Si})_{13}$.

C. Volume fraction of α -Fe, $\text{La}(\text{Fe},\text{Si})_{13}$, and LaFeSi

To quantitatively analyze the influence of solidification conditions on the formation of each phase, a statistical analysis, based on the microstructure results from Figures 1 and 2, of the volume fraction of each phase is conducted. As shown in Figure 4, the volume fraction of $\text{La}(\text{Fe},\text{Si})_{13}$ phase reaches ~50 pct for most directionally solidified alloys, except G1000R100. When the crystal growth rate is 15 or 50 $\mu\text{m}/\text{s}$, there is little LaFeSi phase in all directionally solidified alloys, which implies that a dual-phase microstructure may be achieved by controlling different directional solidification conditions.

Figure 5 indicates the relationship between volume fraction of the $\text{La}(\text{Fe},\text{Si})_{13}$ phase and temperature gradients. With the increase of temperature gradients, the volume fraction of the 1:13 phase becomes further dependent on the growth rate. When the temperature gradient is 300 K/cm, the maximum volume fraction difference of the 1:13 phase is approximately 9 pct when the growth rates increase from 15 to 100 $\mu\text{m/s}$. However, this value reaches 62 pct when the temperature gradient increases to 1000 K/cm, as shown in Figure 5. This is probably due to the large temperature range between the prime $\alpha\text{-Fe}$ phase and La-rich liquid.^[22] Hence, there is a considerable temperature variation in the liquid when the temperature gradient is rather large, which will influence the optimized temperature of nucleation rate of $\alpha\text{-Fe}$ and $\text{La}(\text{Fe},\text{Si})_{13}$. For different crystal growth rates, the rate will affect the duration of phase growth. The volume fraction of $\text{La}(\text{Fe},\text{Si})_{13}$ at different crystal growth rates is likely to show a sharper change with a large temperature gradient.

D. Si Segregation in $\text{La}(\text{Fe},\text{Si})_{13}$

The chemical compositions of all directionally solidified $\text{LaFe}_{11.6}\text{Si}_{1.4}$ specimens are summarized in Table II. The chemical ratio of La to (Fe, Si) is nearly constant for each different alloy. However, the chemical ratio between Fe and Si elements varies significantly with different solidification conditions. There is a significant Si segregation in directionally solidified $\text{LaFe}_{11.6}\text{Si}_{1.4}$ alloys compared with the predicted atomic concentration of 10 pct, as shown in Table II. It should be noted here that the LaFe_{13} does not actually exist because of its positive Gibbs free energy. The existence of Si leads to a stable status so the $\text{La}(\text{Fe},\text{Si})_{13}$ phase can be formed.^[23] Moreover, NaZn_{13} -type $\text{La}(\text{Fe},\text{Si})_{13}$ is likely to exhibit a giant magnetocaloric effect with low Si contents.^[24] This is due to a first-order phase transition from paramagnetic to ferromagnetic.^[8,9] Since the $\text{La}(\text{Fe},\text{Si})_{13}$ phase is usually formed by annealing, no obvious segregation has been found in annealed $\text{La}(\text{Fe},\text{Si})_{13}$ alloys in the previous research.^[25]

To determine the composition variation of main alloying elements, an EDS line scan is made through the prime phase $\alpha\text{-Fe}$ dendrites, as shown in Figure 6. There is a transition area with a length of $\sim 1.5 \mu\text{m}$ from the $\alpha\text{-Fe}$ phase to the $\text{La}(\text{Fe},\text{Si})_{13}$ phase. When the length of the $\text{La}(\text{Fe},\text{Si})_{13}$ phase is over a certain value, the element content will maintain a certain platform value; otherwise, it will show a peak value, such as peak D to F, as shown in Figure 6(c). The transition area is related to the mechanism of the peritectic reaction, which is discussed later. Previous research has reported that supercooling plays an important role in the nucleation competition between $\alpha\text{-Fe}$ and $\text{La}(\text{Fe},\text{Si})_{13}$.^[26] However, the transition area will be dismissed if the large volume fraction of the $\text{La}(\text{Fe},\text{Si})_{13}$ phase in directionally solidified $\text{LaFe}_{11.6}\text{Si}_{1.4}$ alloys is brought about by the nucleation competition, which could imply a different valid mechanism.

IV. DISCUSSION

As shown in Figures 1, 2, and 3, a dual-phase microstructure in directionally solidified $\text{LaFe}_{11.6}\text{Si}_{1.4}$ alloys are usually accompanied by the coarse $\alpha\text{-Fe}$ phase, which is different from annealed alloys made by dissolving the $\alpha\text{-Fe}$ into the matrix $\text{La}(\text{Fe}, \text{Si})_{13}$ phase. XRD results have indicated that the intensity of the prime phase $\alpha\text{-Fe}$ is still stronger, with a large volume fraction of the $\text{La}(\text{Fe}, \text{Si})_{13}$ phase (Figure 3). These results indicate that a coupled growth of the $\alpha\text{-Fe}$ phase and $\text{La}(\text{Fe},\text{Si})_{13}$ phase may occur.

According to Kurz and Kerr's model,^[27] peritectic solidification usually includes three stages, including the peritectic reaction, peritectic transformation, and liquid direct solidification. Once the peritectic phase is formed from the prime phase reacting with the surrounding liquid, the peritectic reaction stops, and the prime phase is transformed into the peritectic phase by solid–solid peritectic transformation. When the temperature reduces below the peritectic temperature (T_p), the peritectic phase will solidify directly from the liquid phase.

Compared with normal solidification, directional solidification, under the condition shown in Table I, actually occurred at a low cooling rate. In this case, $\alpha\text{-Fe}$ will directly form as the prime phase; therefore, the ($\alpha\text{-Fe}$)/liquid interface should be considered. Since La is easily volatilized during solidification, a hypo-peritectic $\text{La}(\text{Fe},\text{Si})_{13}$ alloy is considered in this discussion. Considering the initial component ($\text{La}_{1-\Delta}\text{Fe}_{11.6}\text{Si}_{1.4}$) of $\text{La}(\text{Fe},\text{Si})_{13}$ to be $C_0(T_{\text{initial}})$, when the descending temperature approaches $T_{\text{peritectic}}$:

$$C_L^{*\alpha}(T_{\text{peritectic}}) = C_0(T_{\text{initial}})/k_{0\alpha}. \quad [1]$$

Since $C_0(T_{\text{initial}}) > C_{\alpha}^{\text{per}}(T_{\text{peritectic}})$, it will obtain:

$$C_L^{*\alpha}(T_{\text{peritectic}}) = \frac{C_0(T_{\text{initial}})}{k_{0\alpha}} > \frac{C_{\alpha}^{\text{per}}(T_{\text{peritectic}})}{k_{0\alpha}} = C_L^{\text{per}}(T_{\text{peritectic}}). \quad [2]$$

Hence, prime phase $\alpha\text{-Fe}$ will grow in a meta-stable status. When the supercooling that is required for the formation of $\text{La}(\text{Fe},\text{Si})_{13}$ is attained (Figure 7(a) Point A), the nucleation of $\text{La}(\text{Fe},\text{Si})_{13}$ starts, resulting in the growth of the $\text{La}(\text{Fe},\text{Si})_{13}$ phase and thereby releasing latent heat. In this case, since $\text{La}(\text{Fe},\text{Si})_{13}$ is formed, the interface $\beta(\text{La}(\text{Fe},\text{Si})_{13})/\text{L}$ should be considered (Figure 7(a) Point B). During this process, although the peritectic reaction is blocked, peritectic transformation is still activated by solid–solid diffusion at high temperatures, as shown in Figure 7(b).

Since La-rich liquid is poor in fluidity, the latent heat cannot be easily transferred. The temperature will increase slightly, accompanied by the growth of $\text{La}(\text{Fe},\text{Si})_{13}$. When the temperature is increased to $T_{\text{peritectic}}$, resulting from $C_0(T_{\text{initial}}) < C_{\beta}^{\text{per}}(T_{\text{peritectic}})$, which is similar to the cooling process, it will obtain:

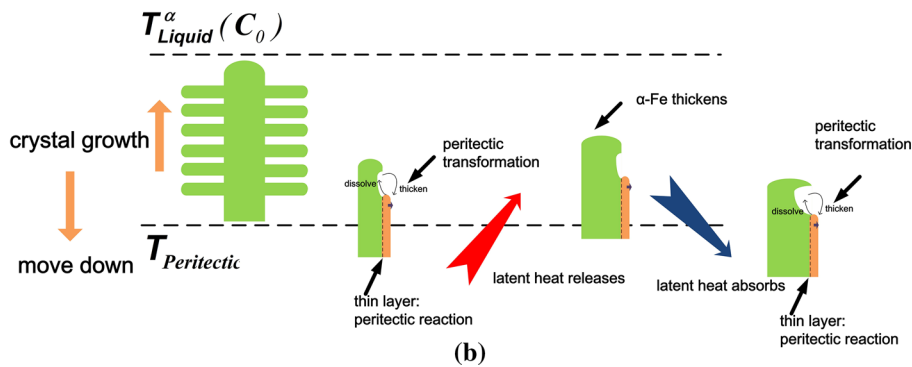
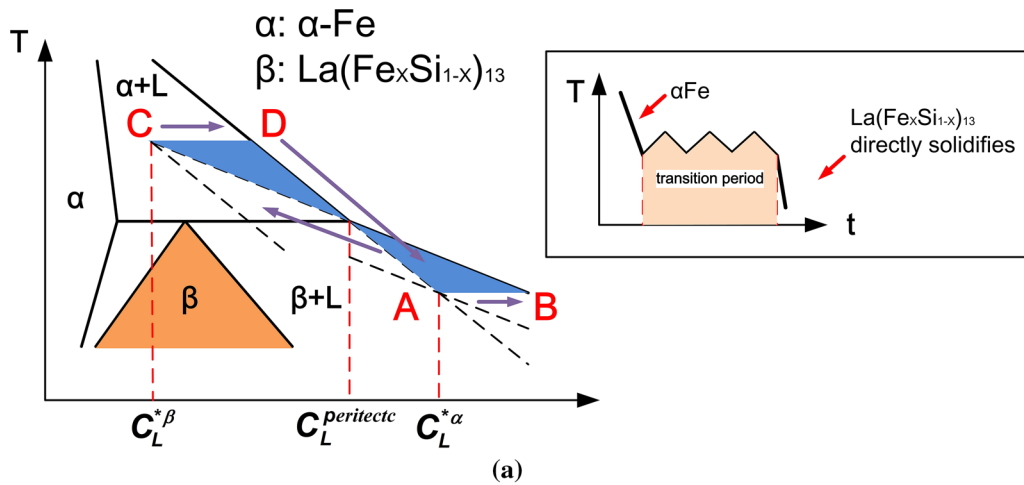


Fig. 7—(a) Since the NaZn_{13} -type structure is directly formed, it is considered as a binary phase diagram between La and (Fe,Si). The mechanism of couple growth of α -Fe phase and $\text{La}(\text{Fe,Si})_{13}$ phase is indicated. The inset figure suggests the temperature variation in three peritectic solidification stages. (b) A schematic of the formation of the large volume fraction of the $\text{La}(\text{Fe,Si})_{13}$ phase.

$$C_L^{*\beta}(T_{\text{peritectic}}) = \frac{C_0(T_{\text{initial}})}{k_{0\beta}} < \frac{C_{\beta}^{\text{per}}(T_{\text{peritectic}})}{k_{0\beta}} = C_L^{\text{per}}(T_{\text{peritectic}}). \quad [3]$$

Hence, it will obtain the supercooling required for the formation of α -Fe (Figure 7(a) Point C), followed by the growth of the α -Fe phase (Figure 7(a) Point D). The coarsening of α -Fe is shown in Figure 7(b). This is in accordance with the existence of the transition area because of the peritectic transformation.

When the temperature is lower than that required to activate peritectic transformation, the liquid is likely to directly solidify to form the $\text{La}(\text{Fe,Si})_{13}$ phase. In this case, the LaFeSi phase is likely to generate in $\text{LaFe}_{11.6}\text{Si}_{1.4}$ alloys with high crystal growth rates and large temperature gradients. For the Si segregation, it is closely connected to the direct liquid solidification.

In general, dual-phase $\text{LaFe}_{11.6}\text{Si}_{1.4}$ alloys are predicted to form in the following ways:

1. Prime phase α -Fe forms first.
2. The $\text{La}(\text{Fe,Si})_{13}$ phase is formed through a peritectic reaction and peritectic transformation, accompanied by the coarsening of the α -Fe phase. The chemical component of the rest liquid will approach $\text{La}(\text{Fe,Si})_{13}$.

3. The rest liquid will directly solidify to form the $\text{La}(\text{Fe,Si})_{13}$ phase.

V. CONCLUSION

1. The volume fraction of the $\text{La}(\text{Fe,Si})_{13}$ phase in La-Fe-Si magnetocaloric alloy can be increased to ~62 pct by ZMLMC directional solidification. The increasing volume fraction of the $\text{La}(\text{Fe,Si})_{13}$ phase was accompanied by the coarsening of the α -Fe phase.
2. A large temperature gradient causes a distinct difference in volume fraction of the $\text{La}(\text{Fe,Si})_{13}$ phase for directionally solidified alloys. In this case, there is no $\text{La}(\text{Fe,Si})_{13}$ phase in the G1000R100 alloy, but for G600R100 and G300R100, a large volume fraction of the $\text{La}(\text{Fe,Si})_{13}$ phase can still be obtained.
3. A significant Si segregation was seen, which can be attributed to a ‘transition area’ observation.
4. The solidification path was discussed according to the peritectic solidification path, which can be used to interpret the increase of the volume fraction of the $\text{La}(\text{Fe,Si})_{13}$ phase by directional solidification.

ACKNOWLEDGMENTS

This work is sponsored by Joint Funds of the National Natural Science Foundation of China. (No. U1660203), National Natural Science Foundation of China (Grant Nos. 51404152 and 51374144), Shanghai Pujiang Program (Grant No. 14PJ1404800), Shanghai International Cooperation Project (Grant No. 14140711000), Shanghai Municipal Natural Science Foundation (13ZR1420600), and Shanghai Rising-Star Program (14QA1402300).

REFERENCES

1. L. Mañosa, A. Planes, and M. Acet: *J. Mater. Chem.*, 2013, vol. 1, pp. 4925–36.
2. X. Moya, S. Kar-Narayan, and N.D. Mathur: *Nat. Mater.*, 2014, vol. 13, pp. 439–50.
3. O. Tegus, E. Brück, K.H.J. Buschow, and F.R. De Boer: *Nature*, 2002, vol. 415, pp. 150–52.
4. B.G. Shen, J.R. Sun, F.X. Hu, H.W. Zhang, and Z.H. Cheng: *Adv. Mater.*, 2009, vol. 21, pp. 4545–64.
5. F.X. Hu, B.G. Shen, J.R. Sun, G.J. Wang, and Z.H. Cheng: *Appl. Phys. Lett.*, 2002, vol. 80, pp. 826–28.
6. A. Fujita, Y. Akamatsu, and K. Fukamichi: *J. Appl. Phys.*, 1999, vol. 85, pp. 4756–58.
7. K. Fukamichi, A. Fujita, and S. Fujieda: *J. Alloy. Compd.*, 2006, vols. 408–412, pp. 307–12.
8. A. Fujita, S. Fujieda, K. Fukamichi, H. Mitamura, and T. Goto: *Phys. Rev. B*, 2001, vol. 65, p. 014410.
9. F.X. Hu, B.G. Shen, J.R. Sun, Z.H. Cheng, G.H. Rao, and X.X. Zhang: *Appl. Phys. Lett.*, 2001, vol. 78, pp. 3675–77.
10. J. Shen, Y.X. Li, Q.Y. Dong, and J.R. Sun: *J. Magn. Magn. Mater.*, 2009, vol. 321, pp. 2336–39.
11. J. Shen, B. Gao, Q.Y. Dong, Y.X. Li, F.X. Hu, and B.G. Shen: *J. Phys. D Appl. Phys.*, 2008, vol. 41, p. 245005.
12. J. Shen, Y.X. Li, J.R. Sun, and B.G. Shen: *Chin. Phys. B*, 2009, vol. 18, pp. 2058–62.
13. Y.F. Chen, F. Wang, B.G. Shen, J.R. Sun, G.J. Wang, F.X. Hu, and Z. Tao: *J. Appl. Phys.*, 2003, vol. 93, pp. 6981–83.
14. Y.F. Chen, F. Wang, B.G. Shen, F.X. Hu, J.R. Sun, G.J. Wang, and Z.H. Cheng: *J. Phys.: Condens. Matter*, 2003, vol. 15, pp. L161–67.
15. P. Lu and H.P. Wang: *Scientific Reports*, 2016, vol. 6, p. 22641.
16. Y. Shao, M. Zhang, H. Luo, A. Yan, and J. Liu: *Appl. Phys. Lett.*, 2015, vol. 107, p. 152403.
17. O. Gutfleisch, A. Yan, and K.H. Müller: *J. Appl. Phys.*, 2005, vol. 97, pp. 10M305(1)–10M305(3).
18. H.N. Beza, C.S. Teixeira, B.G.F. Eggert, J.A. Lozano, M.S. Capovilla, J.R. Barbosa, Jr, and P.A.P. Wendhausen: *IEEE Trans. Magn.*, 2013, vol. 49, pp. 4646–29.
19. H.N. Bez, B.G.F. Eggert, J.A. Lozano, C.R.H. Bahl, J.R. Barbosa, Jr, C.S. Teixeira, and P.A.P. Wendhausen: *J. Magn. Magn. Mater.*, 2015, vol. 386, pp. 125–28.
20. B.M. Ma and C.O. Bounds: *J. Appl. Phys.*, 1991, vol. 70, pp. 6471–73.
21. Y.J. Huang, Q.D. Hu, J. Liu, L. Zeng, D.F. Zhang, and J.G. Li: *Acta Mater.*, 2013, vol. 61, pp. 5702–12.
22. K. Niitsu and R. Kainuma: *Intermetallics*, 2012, vol. 20, pp. 160–69.
23. W.H. Tang, J.K. Liang, G.H. Rao, and X.H. Yan: *Phys. Stat. Sol.*, 1994, vol. 141, pp. 217–22.
24. K.A. Gschneidner, Y. Mudryk, and V.K. Pecharsky: *Scripta Mater.*, 2012, vol. 67, pp. 572–77.
25. S. Fujieda, K. Fukamichi, and S. Suzuki: *J. Alloy. Compd.*, 2013, vol. 566, pp. 196–200.
26. X.L. Hou, P.L. Kelley, Y. Xue, C.Y. Liu, H. Xu, N. Han, C.W. Ma, H. Srikanth, and M.H. Phan: *J. Alloy. Compd.*, 2015, vol. 646, pp. 503–11.
27. H.W. Kerr and W. Kurz: *Int. Mater. Rev.*, 1996, vol. 41, pp. 129–64.